Robotica (2023), **41**, pp. 511–529
doi:10.1017/S0263574722000364

CAMBRIDGE UNIVERSITY PRESS

RESEARCH ARTICLE

SAU-RFC hand: a novel self-adaptive underactuated robot hand with rigid-flexible coupling fingers

Congjia Su[1,2], Rui Wang[1,*], Tao Lu[1] and Shuo Wang[1,2,3]

[1]State Key Laboratory of Management and Control for Complex Systems, Institute of Automation, Chinese Academy of Sciences, Beijing 100190, China, [2]School of Artificial Intelligence, University of Chinese Academy of Sciences, Beijing 100049, China, and [3]Center for Excellence in Brain Science and Intelligence Technology, Chinese Academy of Sciences, Shanghai 200031, China
*Corresponding author. E-mail: rwang5212@ia.ac.cn

Received: 12 June 2021; **Revised:** 20 February 2022; **Accepted:** 23 February 2022; **First published online:** 30 March 2022

Keywords: robot hand, self-adaptive underactuated finger, rigid-flexible structure, contact force distribution

Abstract

In this paper, a novel self-adaptive underactuated robot hand with rigid-flexible coupling fingers (SAU-RFC hand) is proposed. The seven degrees of freedom (DOFs) SAU-RFC hand is driven by four servomotors, consists of three fingers, including two side-turning (ST) fingers and one non-side-turning finger. Specially, the ST fingers can perform synchronous reverse rotation laterally with each other. Each finger with three joints and two DOFs introduces a flexible structure, and the inner part of the proximal phalanx that makes most of the contact with the object is replaced by a flexible belt. The fingers can generate flexion/extension under the pull of the flexible belt, and the middle and distal phalanxes are mechanically coupled through a four-bar linkage. In particular, the flexible belt in the inner direction of the finger will deform, while it will not deform in the outer direction since the outer is a rigid structure. The flexible belt not only plays the role of transmitting power but also has the effect of uniformizing the contact force. Due to the rigid-flexible finger structure, the developed robot hand has a higher self-adaptive grasping ability for objects with different shapes, sizes, and hardness. In addition, the kinematic and kinetic analyses of SAU-RFC hand are performed. A contact force distribution model is established for the flexible belt, which demonstrates its effect of promoting uniform force distribution theoretically. In the end, experiments are conducted on different objects to verify the performance of SAU-RFC hand.

1. Introduction

The end effector has always been a key factor restricting the interaction between the robot and the environment. As a new generation of effector, the multi-finger robot hand has begun to take shape after decades of development, but its dexterity is still far lower than that of a human hand [1–4]. In order to achieve human-like high degree of freedom (DOF) and grasping flexibility, researchers have developed many dexterous multi-fingered hands such as Robonaut hand [5], Shadow hand [6], UBH-3 hand [7], and DLR/HIT hand [8]. However, most of these robot hands adopt the full-actuated method to ensure independent movement of each joint, with high flexibility and control accuracy, but inevitably there are problems such as low system integration, poor environmental compliance, and high cost.

In order to solve these problems, researchers have focused their attention to the underactuated robot hand. The so-called underactuation refers to using fewer actuators to control more joint motions, and there is often a coupling relationship between each joint [9]. The excellent examples are iHY hand [10], SSSA hand [11], PASA-GB hand [12], and BLT hand [13]. Due to the use of fewer actuators, the mechanical structure of the underactuated hand is simplified, which has the characteristics of compact structure, light weight, and convenient control. Compared with the full-actuated hand, the passive joint structure makes it easier to achieve self-adaptive grasping in the grasp mode, self-adaptive grasping has higher environmental compliance and grasping stability, and the grasping range is further expanded.

However, the finger phalanxes of the existing underactuated hands are often rigid, and the grasping method adopts rigid contact [14,15]. During the grasping process, the number of contact points or contact area with the object is small, and the contact force distribution is not uniform, which limits self-adaptive grasping ability. Researchers attempt to improve the contact area between the finger and the object by covering the surface of finger with flexible materials that are easily deformed [16,17]. But the coverage area and thickness of flexible materials are restricted due to limit sizes of the finger, which affects the stability of grasping. In this case, some soft robot hands came into being. Abondance et al. [18] proposed a soft hand with dexterous fingers capable of several basic motion, which can robustly perform in-hand manipulation in the presence of uncertainty. Yang et al. [19] presented a soft gripper based on kirigami shells – thin, elastic shells patterned with an array of cuts. Nevertheless, the grasping power of soft hand is relatively limited, and it is prone to irreversible structural deformation. In addition, some underactuated hands drive the flexion of finger joints through chains or wire ropes [20–23], which can easily cause relaxation, fatigue breakage, and other problems after long-term use.

Therefore, a novel self-adaptive underactuated robot hand with rigid-flexible coupling fingers (SAU-RFC hand) is proposed. The finger motion mechanism is based on the coupling linkage and the flexible belt traction structure. Different from the traditional rigid self-adaptive underactuated hand, the novel finger developed introduces a flexible structure, replacing the inner link of the proximal phalanx with a flexible belt. The flexible belt can be deformed in the inner direction under the action of the traction mechanism and the joint spring, while the outer direction is still a rigid mechanical structure so that it will not be deformed. Due to the rigid-flexible structure, SAU-RFC hand has a higher self-adaptive grasping ability for objects of different shapes, sizes, and hardness. Compared with the high DOF tendon-driven hand, SAU-RFC hand can achieve the same level or even better self-adaptive grasping with lower DOF and simpler mechanical structure by means of the rigid-flexible coupling finger.

In particular, we establish a contact force distribution model of flexible belt to investigate its effect of promoting uniform force distribution. It theoretically indicates that the uniform contact force distribution avoids the stress concentration on a single contact point, which improves the grasping stability. In the end, we perform a series of experiments on different objects to research the grasping performance of SAU-RFC hand. Experiments demonstrate that the novel mechanical design improves the adaptability and stability of dexterous grasping. The main contribution of this paper is the development of a novel rigid-flexible coupling finger and its implement on the self-adaptive underactuated robot hand.

In the reminder of this paper, Section 2 shows the mechanical design of the SAU-RFC hand. The kinematic and kinetic analyses of SAU-RFC hand is given in Section 3. Section 4 presents the experimental results. Finally, the conclusion is summarized in Section 5.

2. Mechanisms and Structure of SAU-RFC Hand

2.1. Design of SAU-RFC finger

Figure 1 illustrates the representative examples of self-adaptive underactuated finger mechanism. Fig. 1(a) is a simplified illustration of the self-adaptive finger described in ref. [9], which is composed of multiple four-bar linkage with two DOFs and one actuation. The structure conforms the object and generates discrete contact forces as the actuation link rotates. This finger is suitable for grasping large payload, but its point contacts apply uneven pressure and may limit range of motion. Another approach is to take advantage of the material's flexibility, as shown in Fig. 1(b), a well-known soft gripper from SRT Co. [24]. This gripper is actuated by air pressure and continuously wraps around the object, distributing the contact force evenly, resulting in a more stable grasp. However, it comes at a cost in terms of grasping position precision and payload capacity. The ideal goal of compliant grasping is to apply uniform force regardless of the size or shape of the object. The concept of typical self-adaptive fingers yields useful inspiration for the development of SAU-RFC finger.

SAU-RFC finger with two DOFs and rigid-flexible coupling structure is shown in Fig. 2. The flexion of finger is achieved by pulling of flexible belt, while the finger is extended by the reverse torque of

https://doi.org/10.1017/S0263574722000364 Published online by Cambridge University Press

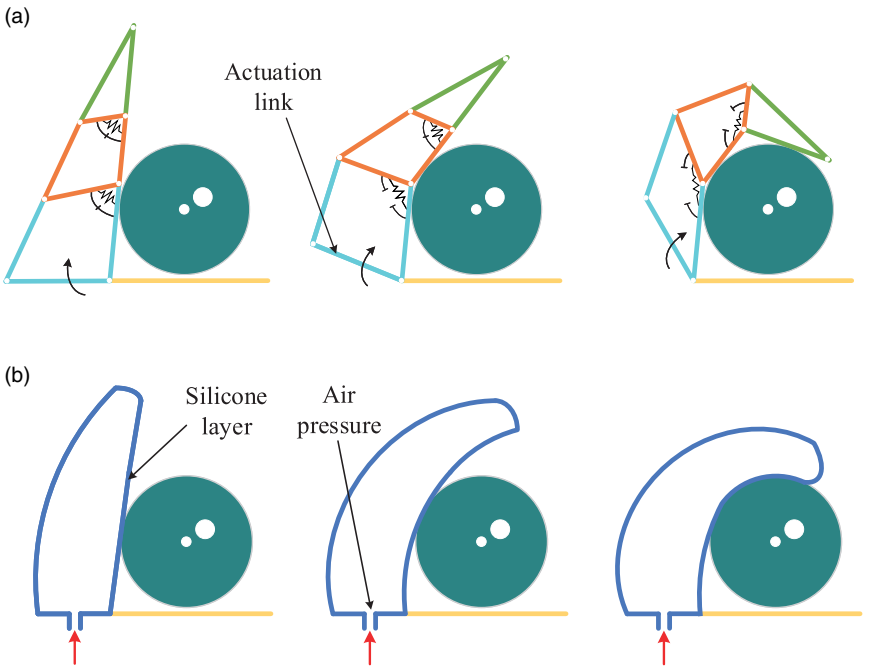

Figure 1. *Conceptual examples of self-adaptive underactuated finger mechanism. (a) A self-adaptive underactuated finger made of multiple four-bar linkages and (b) a soft self-adaptive finger made of silicone.*

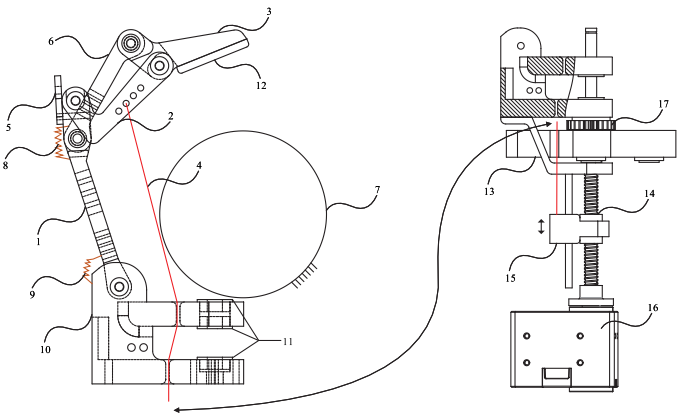

Figure 2. *The mechanical structure of SAU-RFC finger. 1,2,3 – the proximal, middle, and distal phalanx; 4 – the flexible belt; 5 – the limit baffle; 6 – the auxiliary link; 7 – the object; 8 – the middle spring; 9 – the proximal spring; 10 – the finger base; 11 – the bearings; 12 – the soft cover; 13 – the upper base; 14 – the threaded lead screw pair; 15 – the fixer; 16 – the servomotor-I; and 17 – the gear pair.*

the proximal and middle springs. In particular, the elastic coefficient of the middle spring is greater than that of the proximal spring to ensure that the relative position of the three phalanxes remains unchanged before the proximal phalanx touches the object. As the key part of the finger, the first end of flexible belt is connected to the auxiliary link, and the second end crosses the inside of the proximal phalanx and passes through the belt guide path to attach to the external traction mechanism. Note

https://doi.org/10.1017/S0263574722000364 Published online by Cambridge University Press

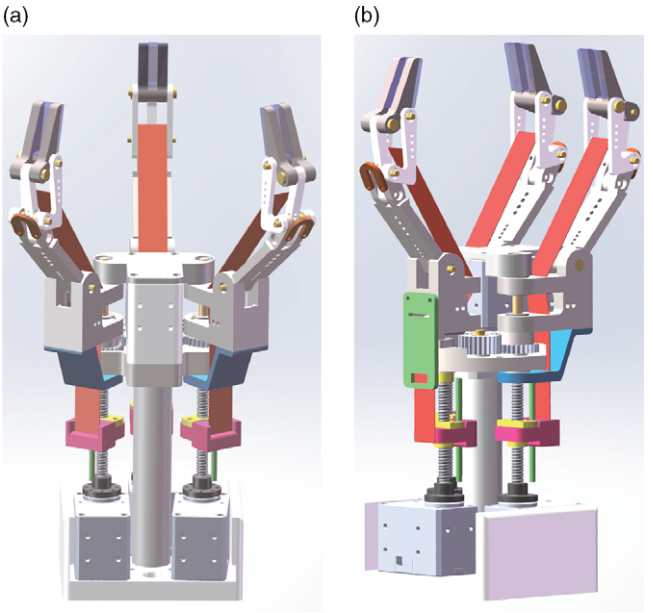

Figure 3. *The SAU-RFC hand. (a) Front view and (b) side view.*

that the flexible belt not only acts as the power transmission carrier to achieve the motion of finger but also acts as a contact surface of object to form a large area envelope contact. Furthermore, it is inevitable that the flexible belt will always suffer from a relaxation problem over time because of its material characteristic. However, the possibility of slack or even breakage of a belt is far less than that of a thread/rope because it is made of interwoven threads. We finally select polyethylene fiber material, which not only has low elongation rate with 5% but also has the features of high wear resistance and high strength.

In addition, the surface of the distal phalanx is also covered with soft material. The traction mechanism is mainly composed of a threaded lead screw pair, a fixer, and a servomotor-I, in which the lead screw is fitted together with the output shaft of servomotor-I, the nut attaches to the first end of fixer, and the second end of fixer is connected to the flexible belt. Based on the connection relationship, the rotary motion of servomotor-I is converted to the pulling motion of belt. Benefiting from the underactuated structure and the actuator is far away from the finger, SAU-RFC finger has a greater advantage in compact design. Due to the flexibility of belt, SAU-RFC finger has high resistance to external shocks and grasping stability.

2.2. Design of SAU-RFC hand

Basing on SAU-RFC Finger, SAU-RFC hand is designed, as shown in Fig. 3. It has three fingers with same structure, a palm base, and four actuators. The palm base has one DOF and is equipped with a side-turning (ST) mechanism. Furthermore, these three fingers can be divided into two ST fingers and one non-side-turning (NST) finger, and the ST fingers can perform synchronous reverse rotation laterally with each other. It is realized by the ST mechanism installed on the palm base, which is composed of a gear pair and a servomotor-II. The gear pair contains an input shaft and two output shafts, and the input shaft is fitted together with the output shaft of servomotor-II, while the output shafts are respectively attached to the corresponding ST fingers. In addition, the rotation angle range of the proximal, the middle, and the distal joint are $0^\circ \sim 100^\circ$, $0^\circ \sim 75^\circ$, and $0^\circ \sim 90^\circ$, respectively. The lateral rotation angle range of ST finger is $0^\circ \sim 60^\circ$. In the interest of matching to the outline of most objects, structural

https://doi.org/10.1017/S0263574722000364 Published online by Cambridge University Press

Table I. *The structure parameters of SAU-RFC hand.*

Item	Parameter
Number of fingers	3
Number of actuators	3
Number of joints	10
Degree of freedom	7
Finger length	118 mm
Finger width	21 mm
Palm base diameter	76 mm
Actuator	Dynamixel servomotor
Flexible belt material	Polyethylene fiber
Weight	0.86 kg
The range of grasping diameter	10 ∼155 mm

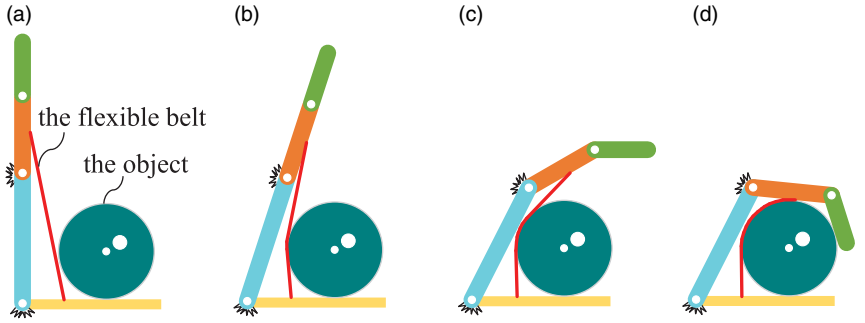

Figure 4. *The grasping process of SAU-RFC finger.*

parameters are selected and modified based on the size of human finger and the extreme position of phalanxes, which are shown in Table I.

2.3. Analysis of grasping process

Figure 4 shows the interaction between a single SAU-RFC finger and the object over the grasping process. Fig. 4(a) is the initial state of the finger, when the grasping action is started, and the flexible belt starts to pull the finger under the action of the traction mechanism. On the one hand, due to the restriction of the middle spring, the middle phalanx will not rotate around the middle joint, and under the influence of the four-bar linkage, the distal phalanx also will not rotate around the distal joint. On the other hand, the elastic coefficient of the middle spring is greater than that of the proximal spring, causing the proximal phalanx rotates around the joint shaft and other phalanxes keep the relative position unchanged.

Therefore, before the finger or the flexible belt touches the object, the entire finger will rotate around the proximal joint to form a larger grasping range, as shown in Fig. 4(b). After the flexible belt contacts the object for the first time, it will automatically deform according to the shape of the object to form an envelope contact with the object. At the same time, due to the obstacle of the object, the proximal phalanx no longer rotates around the proximal joint, but the flexible belt will continue to pull the finger and gradually overcome the resistance of the middle spring. Then, under the effect of the four-bar linkage, the middle and the distal phalanxes are driven to rotate around their joint shaft, respectively, as shown in Fig. 4(c). When the flexible belt continues to pull, each phalanx will automatically adjust its grasping angle according to the shape of the object until the finger reaches a more stable grasping posture, and finally completing the grasping action, as shown in Fig. 4(d), the automatic adjustment of grasping angle also happens to reflect the SAU-RFC finger's self-adaptive effect.

https://doi.org/10.1017/S0263574722000364 Published online by Cambridge University Press

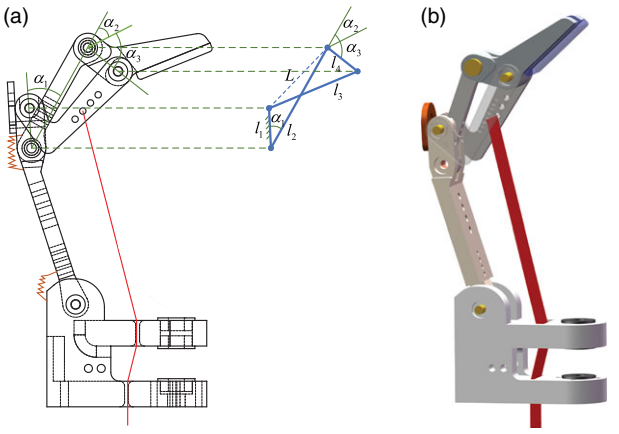

Figure 5. *The four-bar linkage of SAU-RFC finger. (a) 2D view and (b) 3D view.*

In particular, Fig. 5 presents the coupled four-bar linkage between the middle and distal joints, which has the following relationship:

$$\begin{cases} L = \sqrt{l_1^2 + l_2^2 - 2l_1 l_2 \cos\alpha_1} \\ A = \arccos\left(\dfrac{L^2 + l_4^2 - l_3^2}{2Ll_4}\right) \\ B = \arccos\left(\dfrac{L^2 + l_2^2 - l_1^2}{2Ll_2}\right) \\ \alpha_2 = \pi - \alpha_3 - A + B. \end{cases} \tag{1}$$

where, l_1, l_2, l_3, and l_4 are the length of each bar in the four-bar linkage, respectively, α_1 is the rotation angle of the middle joint, α_2 is the rotation angle of the distal joint, and α_3 is the fixed angle determined by the mechanical structure of the distal phalanx.

The motion ratio of α_2 to α_1 and the angle α_3 of the distal phalanx are designed according to the average grasping posture of the human hand. In this way, the change curve for the rotation angle of the distal joint with respect to that of the middle joint is drawn, which have an approximate linear relationship, as shown in Fig. 6. For the convenience of the calculation of inverse kinematics, linear fitting is performed on them (with $R^2 = 0.993$), which is expressed as:

$$\alpha_2 = 0.99\alpha_1 + 6.5. \tag{2}$$

In order to simplify the calculation, the relationship between and can be approximately replaced by Eq. (2).

Moreover, note that the flexible belt forms a large area of contact with the object and has more contact points, which promotes uniform contact force distribution. Under the combined action of the joint spring and the flexible belt, the SAU-RFC finger produces a good self-adaptive grasping effect, which means that it can achieve the enveloping grasp for objects of different shapes and sizes.

3. Kinematic and Kinetic Analyses of SAU-RFC Hand

3.1. Kinematics

As depicted in Fig. 7, the reference frames of each phalanx is established by the Denavit−Hartenberg method. $x_0y_0z_0$ is the fixed coordinate {0} and the others are moving coordinates system. The homogeneous transformation matrix ${}^1A_i^{i-1}(i = 1, 2, 3)$ of the phalanxes for NST finger can be obtained:

https://doi.org/10.1017/S0263574722000364 Published online by Cambridge University Press

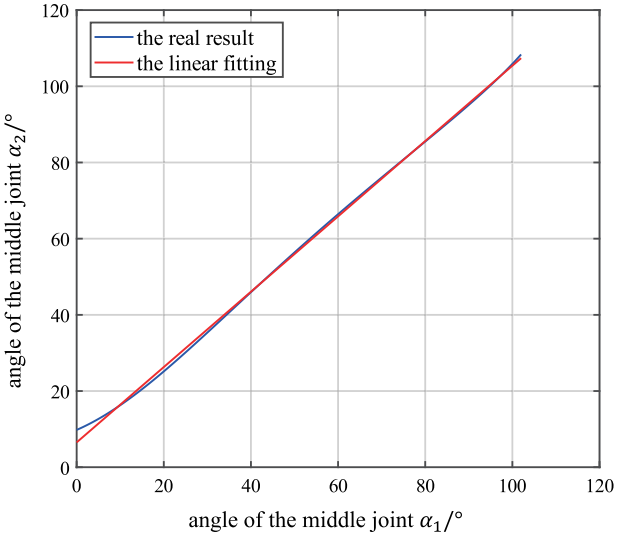

Figure 6. *The grasping process of SAU-RFC finger.*

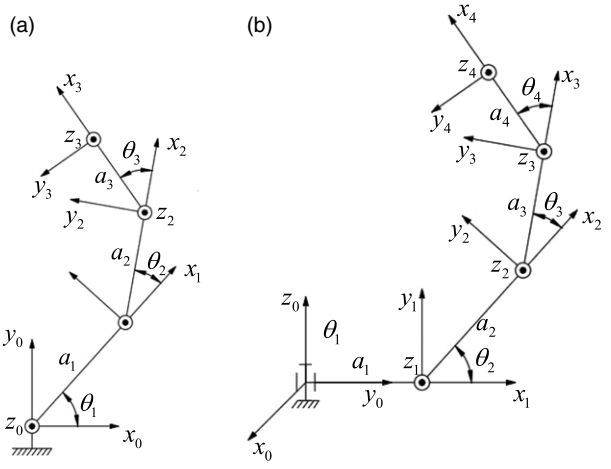

Figure 7. *D-H reference frames of SAU-RFC finger. (a) NST finger and (b) ST finger.*

$$ {}^{1}A_{i}^{i-1} = \begin{bmatrix} \cos\theta_i & -\sin\theta_i & 0 & a_i\cos\theta_i \\ \sin\theta_i & \cos\theta_i & 0 & a_i\sin\theta_i \\ 0 & 0 & 1 & 0 \\ 0 & 0 & 0 & 1 \end{bmatrix}. \tag{3} $$

And the transformation matrix ${}^{2}A_{i}^{i-1}(i = 1, 2, 3, 4)$ of the phalanxes for ST finger are determined by:

$$ {}^{2}A_{1}^{0} = \begin{bmatrix} -\sin\theta_1 & 0 & \cos\theta_1 & -a_1\sin\theta_1 \\ \cos\theta_1 & 0 & \sin\theta_1 & a_1\cos\theta_1 \\ 0 & 1 & 0 & 0 \\ 0 & 0 & 0 & 1 \end{bmatrix} \tag{4a} $$

https://doi.org/10.1017/S0263574722000364 Published online by Cambridge University Press

and

$$ {}^{2}A_{i}^{i-1} = \begin{bmatrix} \cos\theta_i & -\sin\theta_i & 0 & a_i\cos\theta_i \\ \sin\theta_i & \cos\theta_i & 0 & a_i\sin\theta_i \\ 0 & 0 & 1 & 0 \\ 0 & 0 & 0 & 1 \end{bmatrix} \quad i = 2, 3, 4. \tag{4b} $$

Then, the transformation matrix ${}^{1}T_{3}^{0}$ of NST finger's fingertip relative to the coordinate {0} is expressed by:

$$ \begin{aligned} {}^{1}T_{3}^{0} &= {}^{1}A_{1}^{0}\,{}^{1}A_{2}^{1}\,{}^{1}A_{3}^{2} \\ &= \begin{bmatrix} \cos\sum_{i=1}^{3}\theta_i & -\sin\sum_{i=1}^{3}\theta_i & 0 & \sum_{i=1}^{3}\left(a_i\cos\sum_{j=1}^{i}\theta_j\right) \\ \sin\sum_{i=1}^{3}\theta_i & \cos\sum_{i=1}^{3}\theta_i & 0 & \sum_{i=1}^{3}\left(a_i\sin\sum_{j=1}^{i}\theta_j\right) \\ 0 & 0 & 1 & 0 \\ 0 & 0 & 0 & 1 \end{bmatrix}. \end{aligned} \tag{5} $$

Moreover, the transformation matrix ${}^{2}T_{4}^{0}$ of the ST finger's fingertip relative to the coordinate {0} is calculated as:

$$ \begin{aligned} {}^{2}T_{4}^{0} &= {}^{2}A_{1}^{0}\,{}^{2}A_{2}^{1}\,{}^{2}A_{3}^{2}\,{}^{2}A_{4}^{3} \\ &= \begin{bmatrix} -\sin\theta_1\cos\sum_{i=2}^{4}\theta_i & \sin\theta_1\sin\sum_{i=2}^{4}\theta_i & \cos\theta_1 & -\sin\theta_1\left(\sum_{i=2}^{4}\left(a_i\cos\sum_{j=2}^{i}\theta_j\right)+a_1\right) \\ \cos\theta_1\cos\sum_{i=2}^{4}\theta_i & -\cos\theta_1\sin\sum_{i=2}^{4}\theta_i & \sin\theta_1 & \cos\theta_1\left(\sum_{i=2}^{4}\left(a_i\cos\sum_{j=2}^{i}\theta_j\right)+a_1\right) \\ \sin\sum_{i=2}^{4}\theta_i & \cos\sum_{i=2}^{4}\theta_i & 0 & \sum_{i=2}^{4}\left(a_i\sin\sum_{j=2}^{i}\theta_j\right) \\ 0 & 0 & 0 & 1 \end{bmatrix}. \end{aligned} \tag{6} $$

Specifically, for the NST finger, the matrix ${}^{1}T_{3}^{0}$ is the function of joint variables $\theta_i (i = 1, 2, 3)$ (Eq. 5), and the pose of fingertip in the coordinate {0} is expressed as the first three values in the last column of ${}^{1}T_{3}^{0}$. Hence, the pose of fingertip is solved by measuring the value of variables $\theta_i (i = 1, 2, 3)$, as mentioned in Section 2, θ_2 and θ_3 have a linear relationship (Eq. 2), so it is determined by the variables $\theta_i (i = 1, 2)$. Similar analysis can be done for ST finger. Figure 8 presents the workspaces of NST and ST fingers' fingertip, and it is observed that the SAU-RFC hand has a large workspace.

3.2. Kinetics

Once the flexible belt of SAU-RFC finger touches the object, it will cause several contact forces in different orientations and sizes. It is complicated to analyze these forces one by one. Therefore, the composition of forces is adopted to make all the component forces of object to the flexible belt synthesize an equivalent force at the midpoint of the flexible belt. For the convenience of analysis, assuming that the outline of the object being grasped is cylindrical. The grasping force diagram of SAU-RFC finger is shown in Fig. 9, where,

f_1 – the equivalent external force on the proximal phalanx (or the flexible belt), N;

f_2, f_3 – the external force on the middle and distal phalanxes, N;

https://doi.org/10.1017/S0263574722000364 Published online by Cambridge University Press

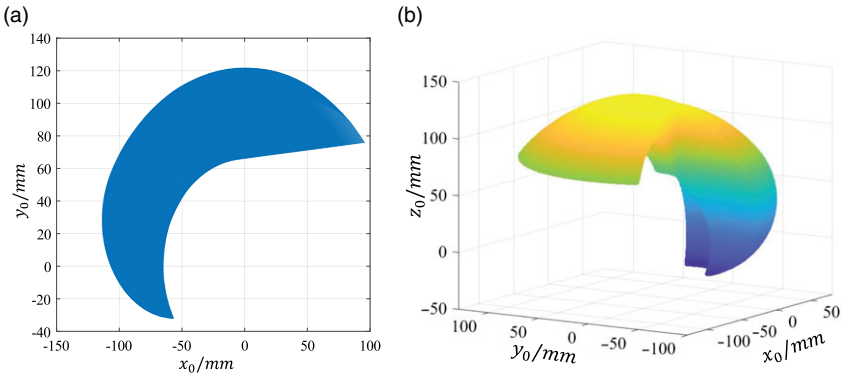

Figure 8. *The workspace of SAU-RFC fingers' fingertip. (a) NST finger and (b) ST finger.*

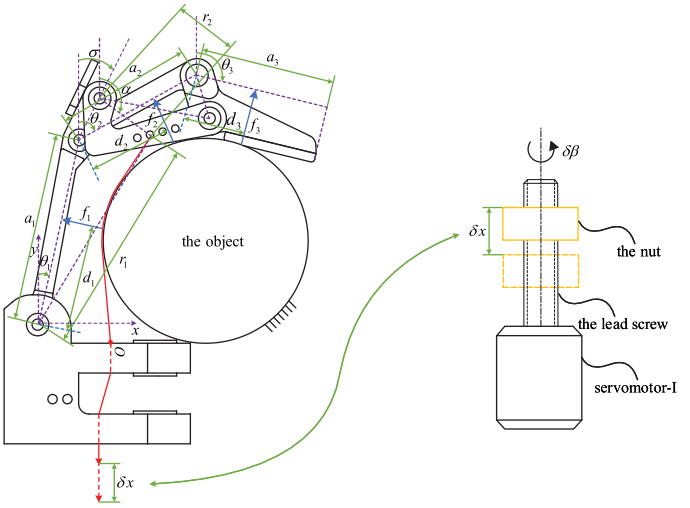

Figure 9. *The grasping force diagram of SAU-RFC finger.*

$\theta_1, \theta_2, \theta_3$ – the rotation angle of the proximal, middle, and distal phalanxes, °; note that θ_2 and θ_3 are associated with α_1 and α_2 in Eq. 2: $\alpha_2 = \theta_3 - \theta_2, \alpha_1 = \theta_2 - \sigma$.

a_1, a_2, a_3 – the length of the proximal, middle, and distal phalanxes, mm;

d_1, d_2, d_3 – the distance between the joint shaft and the force contact point of the proximal, middle, and distal phalanxes, respectively, mm;

T_m – the output torque of servomotor, N · mm;

β – the rotation angle of servomotor, °;

α – the rotation angle of l_3-bar in the four-bar linkage relative to the proximal phalanx, °;

r_1, r_2 – the distance between the first end of the flexible belt and the proximal phalanx joint shaft, and the l_3-bar shaft, respectively, mm;

M_1, M_2 – the initial torque of the proximal and middle spring, N · mm;

k_1, k_2 – the stiffness coefficient of the proximal and middle spring, N · mm/°.

The middle and the distal phalanxes are coupling connected by the four-bar linkage, then f_2 and f_3 are determined by:

$$f_2 d_2 = f_3 \left(d_3 + a_2 \cos\theta_3\right). \tag{7}$$

Then the expression between the force and position is calculated from the principle of virtual work:

https://doi.org/10.1017/S0263574722000364 Published online by Cambridge University Press

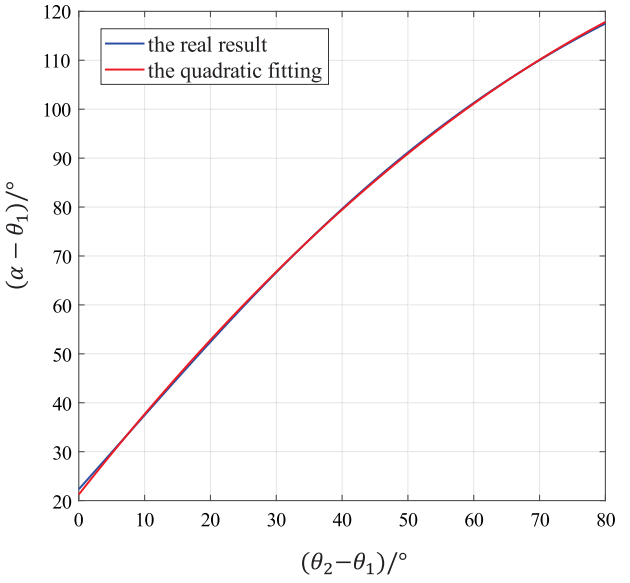

Figure 10. *The relationship between α and θ_2.*

$$\begin{bmatrix} f_1 & f_2 \end{bmatrix} \begin{bmatrix} -d_1 & 0 \\ K & N \end{bmatrix} \begin{bmatrix} \delta\theta_1 \\ \delta\theta_2 \end{bmatrix} = \begin{bmatrix} k_1\theta_1 + M_1 & k_2\theta_2 + M_2 & -T_m \end{bmatrix} \begin{bmatrix} \delta\theta_1 \\ \delta\theta_2 \\ \delta\beta \end{bmatrix}. \tag{8}$$

where, $K = -a_1\cos(\theta_2 - \theta_1) - \dfrac{d_2 a_1 \cos(\theta_3 - \theta_2 - \theta_1) - d_2 d_3}{d_3 + a_2\cos\theta_3}$ and $N = -d_2 - \dfrac{d_2 a_2 \cos(\theta_3 - \theta_2) + 2d_2 d_3}{d_3 + a_2\cos\theta_3}$.

In addition, $\delta\beta$, $\delta\theta_1$, and $\delta\theta_2$ have the following conversion relationship:

$$\begin{cases} \delta\beta/360 = \delta x/s \\ \quad \delta x \approx r_1\delta\theta_1 + r_2\delta\alpha \\ \alpha - \theta_1 = -0.007\,(\theta_2 - \theta_1)^2 + 1.7\,(\theta_2 - \theta_1) + 21 \\ \quad \delta\alpha = (-0.014\,(\theta_2 - \theta_1) + 1.7)\,\delta\theta_2 + (0.014\,(\theta_2 - \theta_1) - 1.7)\,\delta\theta_1. \end{cases} \tag{9}$$

where δx is the tiny reduction of flexible belt and s is the lead of the lead screw pair. Function $\alpha(\theta_2)$ is obtained by quadratic fitting based on the geometric parameters, as shown in Fig. 10. Then the right half of Eq. (8) is expressed as:

$$\begin{bmatrix} k_1\theta_1 + M_1 & k_2\theta_2 + M_2 & -T_m \end{bmatrix} \begin{bmatrix} 1 & 0 \\ 0 & 1 \\ P & Q \end{bmatrix} \begin{bmatrix} \delta\theta_1 \\ \delta\theta_2 \end{bmatrix}. \tag{10}$$

where $P = 360\,(r_1 + r_2\,(0.014(\theta_2 - \theta_1) - 0.7))/s$ and $Q = 360 r_2\,(-0.014(\theta_2 - \theta_1) + 1.7)/s$. Substituting Eq. (10) into Eq. (8) yields

$$\begin{bmatrix} f_1 & f_2 \end{bmatrix} = \begin{bmatrix} k_1\theta_1 + M_1 & k_2\theta_2 + M_2 & -T_m \end{bmatrix} \begin{bmatrix} -\dfrac{1}{d_1} & 0 \\ \dfrac{K}{d_1 N} & \dfrac{1}{N} \\ \dfrac{KQ}{d_1 N} - \dfrac{P}{d_1} & \dfrac{Q}{N} \end{bmatrix}. \tag{11}$$

https://doi.org/10.1017/S0263574722000364 Published online by Cambridge University Press

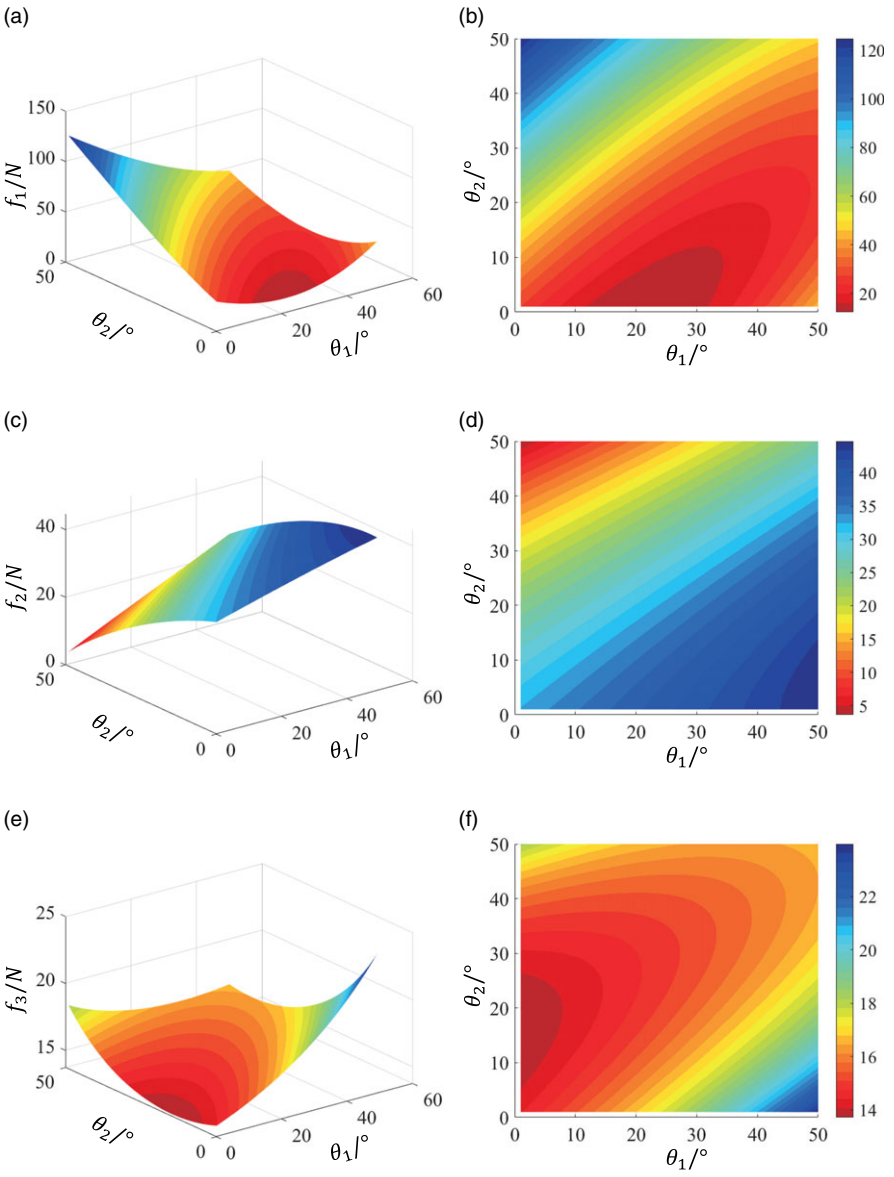

Figure 11. *The relationship between the grasping force and the rotation angle of joints.*

Finally, assuming the necessary parameters: $k_1 = 0.05\,\mathrm{N}\cdot\mathrm{mm}/^\circ$, $k_2 = 0.14\,\mathrm{N}\cdot\,\mathrm{mm}/^\circ$, $a_1 = 51\,\mathrm{mm}$, $a_2 = 36\,\mathrm{mm}$, $d_1 = 25\,\mathrm{mm}$, $d_2 = 22\,\mathrm{mm}$, $d_3 = 14\,\mathrm{mm}$, $T_m = 1\,\mathrm{N}\cdot\mathrm{mm}$, $M_1 = 0.2\,\mathrm{N}\cdot\mathrm{mm}$, $M_1 = 0.54\,\mathrm{N}\cdot\mathrm{mm}$, $r_1 = 59\,\mathrm{mm}$, and $r_2 = 16\,\mathrm{mm}$. The relationship between the grasping force and the rotation angle of the proximal, middle, and distal phalanxes is illustrated in Fig. 11, in which the left column is the 3D view and the right column is the corresponding 2D view. In this figure, the first row is the 3D view of the grasping force, while the second row is the corresponding 2D view. Figure 11 indicates that when θ_1 increases, the grasping force of f_1 the proximal phalanx decreases, while the grasping forces f_2 of the middle phalanx and f_3 of the distal phalanx increase. When θ_2 increases, the grasping force f_1 gradually increases, while the grasping forces f_2 and f_3 gradually decrease. This is because the elastic force of the spring will increase with the increase of joint angle, and the three phalanxes share the power of the servomotor-I, while its output torque is constant.

https://doi.org/10.1017/S0263574722000364 Published online by Cambridge University Press

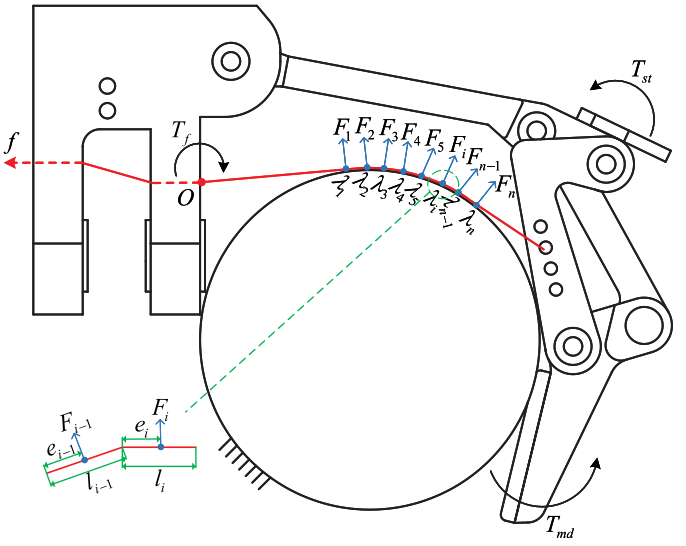

Figure 12. *The model of contact force distribution.*

3.3. Contact force distribution model of flexible belt

In order to further study the change in the contact force distribution caused by replacing the rigid proximal phalanx with the flexible belt, a contact force distribution model is established. As shown in Fig. 12, the flexible belt is regarded as a rigid serial multilink with n joints, which is cut and subdivided into $n+1$ phalanx units. The joints are numbered in the order from 1 to n, and the phalanx units are numbered in the order from 0 to n. The joint i connects the unit $i-1$ and the unit i and drives the unit i. The phalanx unit 0 is fixed, which is equivalent to the "base" of the flexible belt, while each of the remaining phalanx units forms a contact force with the object, that is, $F_1, F_2, F_3, \cdots, F_n$.

To simplify the calculation, let each force form a torque at point O and define some parameters of the finger as follows:

T_i – the moment caused by the contact force F_i on phalanx unit i, N · mm;
T_f – the equivalent moment caused by the tension f of flexible belt, N · mm;
T_{md} – the equivalent moment caused by the contact force on middle and distal phalanxes, N · mm;
T_{st} – the equivalent moment caused by the elastic force of proximal and middle springs, N · mm;
l_i – the length of phalanx unit i, mm;
e_i – the distance between acting point of contact force F_i and joint i, mm;
λ_i – the rotation angle of joint i relative to joint $i-1$, °.
Then, establish the moment equilibrium of flexible belt:

$$\begin{aligned} T_f = {} & T_{md} + T_{st} + F_1 e_1 + F_2 \left(e_2 + l_1 \cos\lambda_2\right) + F_3 \left(e_3 + l_2 \cos\lambda_3 + l_1 \cos\left(\lambda_3 + \lambda_2\right)\right) \\ & \cdots + F_n \left(e_n + l_{n-1} \cos\lambda_n + l_{n-2} \cos\left(\lambda_n + \lambda_{n-1}\right) + \cdots + l_1 \cos\left(\lambda_n + \lambda_{n-1} + \cdots + \lambda_2\right)\right). \end{aligned} \tag{12}$$

By introducing T_i, the above equation is further expressed as:

$$\begin{cases} T_f = \sum_{i=1}^{n} T_i + T_{md} + T_{st} \\ T_i = F_i \left(e_i + l_{i-1} \cos\lambda_i + l_{i-2} \cos\left(\lambda_i + \lambda_{i-1}\right) + \cdots + l_1 \cos\left(\lambda_i + \lambda_{i-1} + \cdots + \lambda_2\right)\right). \end{cases} \tag{13}$$

The value of n is close to infinity and the material of flexible belt is uniform, then the length of each phalanx unit can be regarded as the same. Meanwhile, assuming the contact point of each phalanx unit i

https://doi.org/10.1017/S0263574722000364 Published online by Cambridge University Press

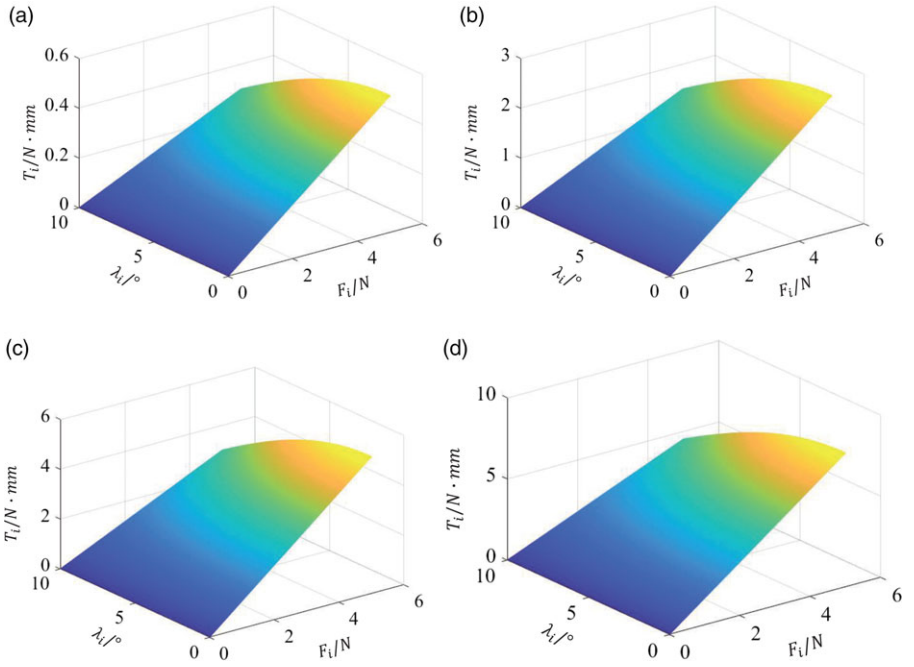

Figure 13. *The relationship between the parameter T_i and F_i, λ_i. (a) $l_i = 0.01$ mm; (b) $l_i = 0.05$ mm; (c) $l_i = 0.10$ mm; and (d) $l_i = 0.15$ mm.*

to the object is at the joint $i + 1$, and the flexible belt takes an arc-shaped grasping posture, that is,

$$\begin{cases} l_1 = l_2 = \cdots = l_n \\ e_i = l_i \\ \lambda_1 = \lambda_2 = \cdots = \lambda_n. \end{cases} \tag{14}$$

Thus, Eq. (13) is calculated as:

$$T_i = F_i \left(e_i + l_i \cos\lambda_i + l_i \cos(2\lambda_i) + \cdots + l_i \cos\left((i-1)\,\lambda_i\right)\right). \tag{15}$$

Aiming at the four cases where l_i is 0.01, 0.05, 0.10, and 0.15mm, respectively, the relationship between T_i and the parameter F_i, λ_i is plotted in Fig. 13. For the length parameter l_i of phalanx unit, Fig. 13(a)−(d) show that T_i increases when l_i increases from 0.01 to 0.15 mm, and its maximum value increases from about 0.5 to 8 N · mm. Therefore, when l_i is small enough, the contact moment of flexible belt can be lower than 0.5 N · mm, and the difference in contact force among phalanx units is also smaller, which means that the flexible belt has a more uniform force distribution than the traditional rigid finger structure.

Meanwhile, every subgraph in Fig. 13 shows that T_i increases with the increase of F_i, while T_i decreases with the increase of λ_i. It indicates that a higher flexible belt contact moment is required when grasping the large-mass and large-volume object than grasping the small-mass and small-volume object, which means that enveloping grasp (power grasp) requires a higher driving torque than pinching grasp (precise grasp).

4. Experiments and Discussion

4.1. Experiments of grasping mode

In order to illustrate the rationality of the mechanical structure, a series of grasping experiments on SAU-RFC hand are performed. The prototype of SAU-RFC hand and its various grasping configurations are shown in Fig. 14. SAU-RFC hand is made of mixed materials such as resin (white part) and nylon

https://doi.org/10.1017/S0263574722000364 Published online by Cambridge University Press

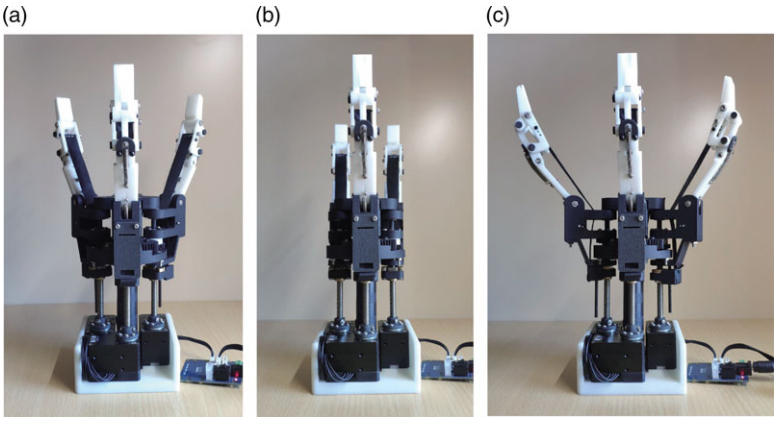

Figure 14. *The prototype and grasping configuration of SAU-RFC hand. (a) configuration-I; (b) configuration-II; and (c) configuration-III.*

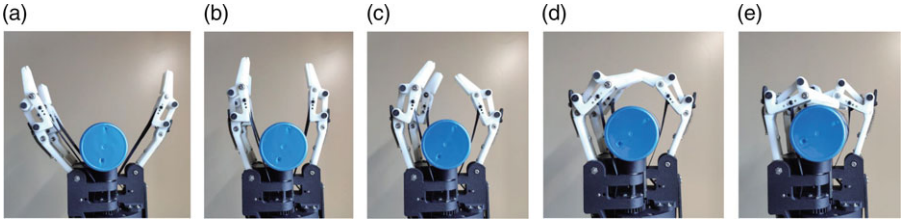

Figure 15. *The enveloping grasp process of SAU-RFC hand.*

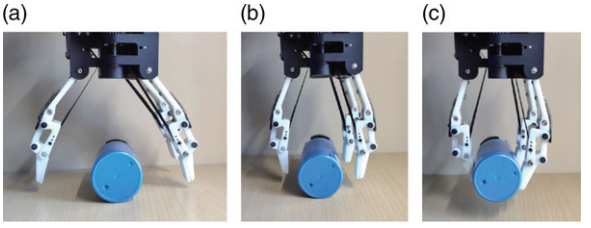

Figure 16. *The pinching grasp process of SAU-RFC hand.*

(black part). Remark that it can automatically select the grasping mode according to the distance of objects from the palm: enveloping grasp or pinching grasp.

When the object is close to the palm, enveloping grasp is performed, which is shown in Fig. 15. As is to see, before touching the object, the three phalanxes rotate around the proximal joint at a constant relative angle, after the proximal phalanx touches the object first, the middle and distal phalanxes start to rotate under the action of the self-adaptive mechanism until they contact the object. Note that each phalanx automatically adjusts its angle according to the contour of object until the fingers reach a more stable grasping posture, which just reflects the self-adaptivity.

When the object is far from the palm, consecutive snapshots of pinching grasp are given in Fig. 16. The middle spring makes the middle and distal phalanxes remain upright, so that SAU-RFC hand can pinch the object tightly. Meanwhile, the soft cover on the surface of the distal phalanx increases the friction.

4.2. Experiments of grasping objects

The grasping versatility of SAU-RFC hand is verified on set of objects to include the flexible belt affects grasping performance, considering the grasping benchmark from other studies. It is mainly based on

https://doi.org/10.1017/S0263574722000364 Published online by Cambridge University Press

Table II. *Statistics of unsuccessful grasping results of SAU-RFC hand.*

Item	Number of successful grasps/total grasps	Item	Number of successful grasps/total grasps
Mug	6/10	Lid	0/10
Soy milk bottle	7/10	Ruler	0/10
Cube model	6/10	Pen	0/10
Triangle model	5/10	Disc	0/10
Electronic key	4/10	Iron plate	0/10
A piece of watermelon	5/10	Meal plate	0/10
Screwdriver	8/10	Tablet-1	0/10
Little papaya	7/10	Tablet-2	0/10
Hammer	6/10	Sponn	0/10
Gear	3/10	Little orange	0/10
Wrench	0/10	Little pear	0/10
Key	0/10	Clump weight (2.8 kg)	0/10

Figure 17. *Examples of SAU-RFC hand grasping various objects from the YCB object set.*

the Yale-CMU-Berkeley (YCB) object set [25], which comprises 60 objects in 5 categories, including food items and tools.

Often, there is variation added to the object position and orientation in the realistic pick-and-place environment, which is more representative of practical applications. Therefore, experiment is conducted with YCB benchmark involving 60 unique objects grasped 10 times in random object orientation, as shown in Fig. 17. This figure also presents how the rotation of ST fingers and the grasping mode (pinching grasp/enveloping grasp) is employed to help grasp objects depending on their geometry. During the 10 times of grasping, the random placement of objects will cause some unsuitable orientations, resulting in the grasping failure, and the unsuccessful results are summarized in Table II.

SAU-RFC hand successfully grasped the majority of the objects only failing on the smaller flat objects and the heavier ones, and the successful/ unsuccessful objects are shown in Fig. 18. The effectiveness

https://doi.org/10.1017/S0263574722000364 Published online by Cambridge University Press

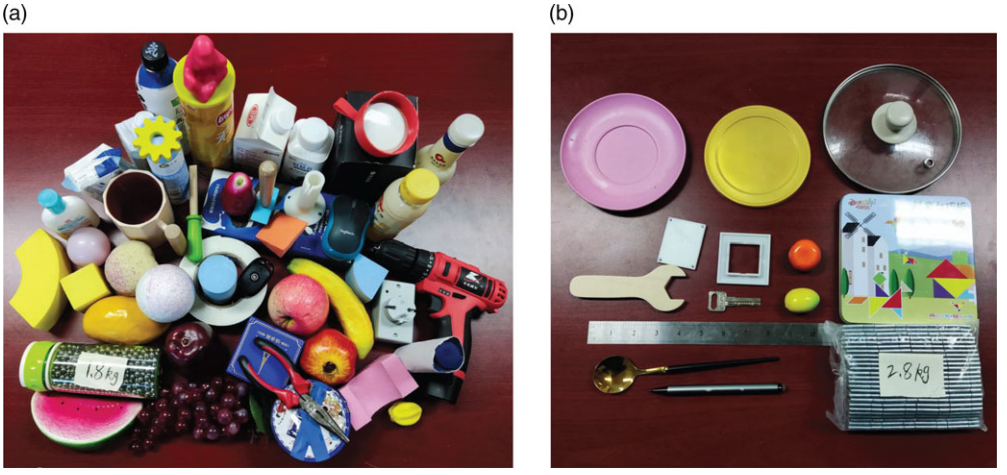

Figure 18. *(a) Items from the YCB object set that the SAU-RFC hand was able to grasp in 10 times and (b) items from the YCB object set that the SAU-RFC hand was unable to grasp in 10 times.*

of pinching grasp is proved on small objects, and enveloping grasp can hold the object tightly for large objects. Overall, SAU-RFC hand has the ability to grasp objects of various shapes self-adaptively benefiting from the compliance of belt. But the flat objects prove a significant challenge for this hand, because it is no suitable grasping posture to match the narrow edge of flat objects. Similarly, the flexibility of the flexible belt results in power grasp being more subject to failure when facing sharp or heavy (more than 2.8 kg) objects. Nevertheless, it does show the physical properties of objects that the SAU-RFC hand is likely to struggle with, indicating limitations in the design.

4.3. Validation of grasping stability

Stability is an important indicator to measure the grasping capability of the robot hand; thus, disturbance experiments are carried out after grasping by introducing random perturbations in the hand pose and external collision. The hand pose is perturbed by shaking the object to the same degree from random directions. Figure 19 shows the snapshot of perturbation in the hand pose after grasping different objects. The left column is the selected four objects, which are cylinder bottle, electric drill, stapler, and multimeter from top to bottom, while the right column is the video sequence of the object state. The tests show that object weighing below 2.8 kg can be grasped without sliding even when disturbed by random hand pose, which demonstrates good stability.

The external collision is caused by a bottle falling freely at different heights and hitting the fixed position of the hand in a positive direction. Specifically, SAU-RFC hand holding the object is placed horizontally, a 400 g bottle is freely fallen within a height of $20 - 80$ cm above it, and the initial height is recorded when the object slips off. Experiment presents that the fingers are severely deformed and the object slips off when the bottle falls freely about 45 cm above the hand and calculate the impulse value as 1.19 kg · m/s by momentum theorem, indicating SAU-RFC finger has high resistance to external shocks. If the fingers are fabricated by stronger material, the impulse will be higher. Overall, the experiments demonstrate that the novel mechanical design of the SAU-RFC hand has a good adaptability and stability of grasping.

4.4. Discussion

The famous three-finger underactuated hands in the robot hand community include Robotiq hand [26], iHY hand [10], Barrett hand [27], DSR hand [18], and so forth, SAU-RFC hand is different from them in technical characteristics such as driving type, which are compared in Table III. It is worth noting

https://doi.org/10.1017/S0263574722000364 Published online by Cambridge University Press

Table III. *Comparison of SAU-RFC hand with other designs.*

The hand	Robotiq hand [26]	iHY hand [10]	Barrett hand [27]	DSR hand [18]	SAU-RFC hand
Driving type	Link driven	Tendon driven	Gear+belt driven	Pneumatic driven	Belt driven
Degree of freedom	6	7	7	6	7
Number of joints in a single finger	3	2	2	2	3
The distribution of contact point	Nonuniform	Nonuniform	Nonuniform	Nonuniform	Uniform
Ability to resist external shocks	Weak	Medium	Weak	Weak	Strong
Softness of finger	Rigid	Rigid	Rigid	Soft	Rigid-flexible coupled

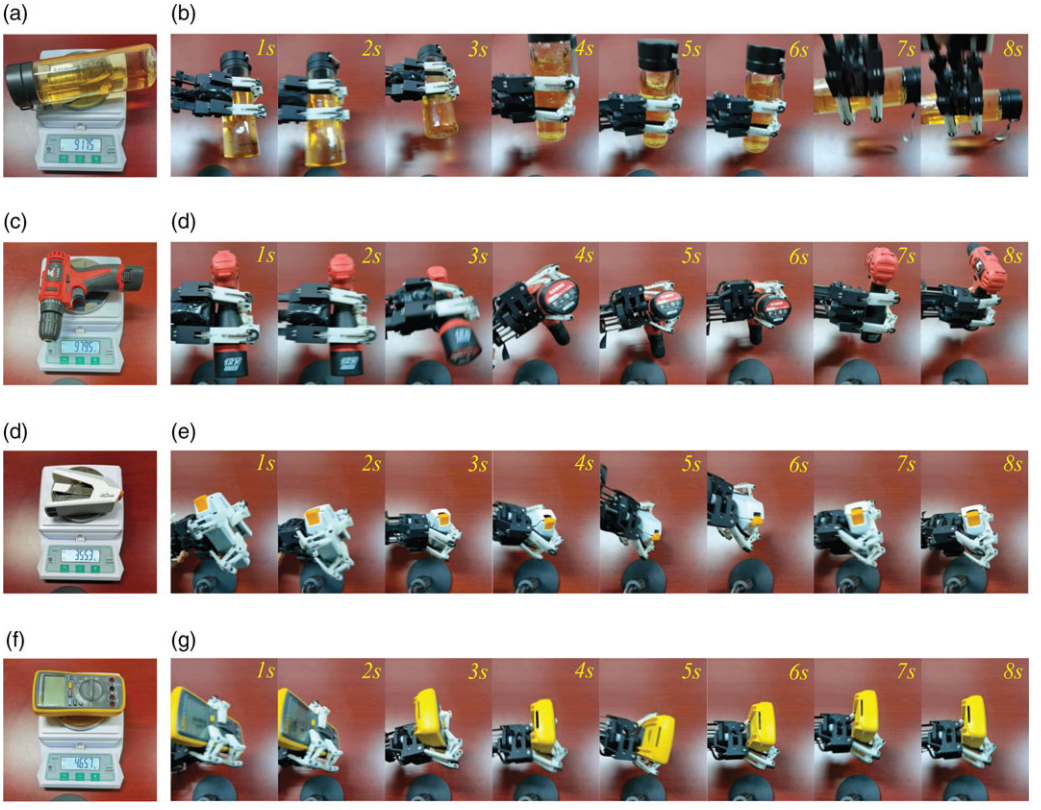

Figure 19. *Disturbance experiments after grasping different objects with SAU-RFC hand.*

that the SAU-RFC hand is belt-driven and rigid-flexible coupled. This enables remarkable robustness and grasping stability in the face of external impact at the expense of a certain level of precision, which is in stark contrast to the design philosophy of other hands. Additionally, when the rigid-flexible coupling finger is deployed, SAU-RFC hand provides a uniform contact force across a surface, rather than concentrating it on a point or line, which is a desirable property for grasping that is compliant.

https://doi.org/10.1017/S0263574722000364 Published online by Cambridge University Press

However, SAU-RFC hand has some limitations in its application, which include

1. *The small flat, the heavier, or the sharp objects.* The small flat objects present a significant challenge for this hand, as there is no grasping posture that corresponds to the narrow edge. The heavier objects (more than 2.8 kg) will exceed the load-bearing limit of the fingers. Additionally, the belt's flexibility makes the power grasp more susceptible to failure when confronted with sharp objects, as sharp objects such as knives may pierce the belt.
2. *Within-hand manipulation.* The design of SAU-RFC hand focuses on grasping, not manipulation. SAU-RFC finger is driven by a flexible belt, performs self-adaptive grasping using the elastic difference between the proximal and middle joint springs, and adaptively adjusts the joint angles to the contour of the object. Due to the difficulty of precisely controlling the angle of each joint, SAU-RFC hand is not particularly adept at manipulating objects.
3. *Fatigue damage.* Due to the material characteristics of the flexible belt, it is unavoidable that it will suffer from a relaxation problem over time. However, because a belt is made of interwoven threads, the possibility of slack or even breakage is significantly less than that of a thread/rope.

5. Conclusion and Future Work

The development of a novel self-adaptive underactuated robot hand named SAU-RFC hand has been presented, and its flexible grasping operation has been achieved. In the design of mechanical structure, the finger mechanism is based on the rigid-flexible structure and the coupling four-bar linkage. Specially, different from the traditional robot hands with rigid phalanxes, a flexible belt is introduced so that the nonuniformity of force distribution is refined. Due to the self-adaptive mechanism, SAU-RFC hand can efficiently coordinate the modes of enveloping grasp and pinching grasp. Moreover, the kinematic and kinetic analyses of SAU-RFC hand are given. Furthermore, a contact force distribution model is also established to evaluate the grasping stability. Physical experiments are conducted to verify that SAU-RFC hand has great self-adaptive grasping performance and strong grasping versatility.

In the future, we will increase the DOF of robot palm to enrich the grasping posture, develop and integrate a fingertip visuotactile sensor to perceive tactile information, and ultimately realize human-like dexterous grasping in unstructured environments. In addition, representation learning methods to extract features from visual and tactile spatiotemporal sequences will also be researched.

Acknowledgement. This work was supported in part by the National Key Research and Development Program of China under Grant 2019YFB1311901, in part by the National Natural Science Foundation of China under U1913201, in part by the Beijing Nova Program under Grant Z211100002121152, in part by the Beijing Natural Science Foundation under Grant 4222056, and in part by the Youth Innovation Promotion Association CAS under Grant 2020137.

Authors' Contributions. *Congjia Su*: conceptualization, methodology, investigation, data curation, and writing – original draft. *Rui Wang*: software, resources, project administration, supervision, funding acquisition, writing – review, and editing. *Tao Lu*: visualization, investigation, and validation. *Shuo Wang*: software, supervision, funding acquisition, writing – review, and editing.

Conflict of Interest. Authors have no conflict of interest to declare.

Ethical Standards. Authors have no ethical considerations to declare.

References

[1] A. Billard and D. Kragic, "Trends and challenges in robot manipulation," *Science* **364**(6446), 370 (2019).
[2] H. Kawasaki and T. Mouri, "Humanoid robot hand and its applied research," *J. Robot. Mechatron.* **31**(1), 16–26 (2019).
[3] J. Vertongen, D. Kamper, G. Smit and H. Vallery, "Mechanical aspects of robot hands, active hand orthoses and prostheses: A comparative review," *IEEE/ASME Trans. Mechatron.* **26**(2), 955–965 (2021).

https://doi.org/10.1017/S0263574722000364 Published online by Cambridge University Press

[4] D. Xu and Q. Wang, "Noninvasive human-prosthesis interfaces for locomotion intent recognition: A review," *Cyborg Bionic Syst.* **2021**(2), 1–14 (2021).
[5] R. O. Ambrose, H. Aldridge, R. S. Askew, R. R. Burridge, W. Bluethmann, M. Diftler, C. Lovchik, D. Magruder and F. Rehnmark, "Robonaut: NASA's space humanoid," IEEE Intell. Syst. Their Appl. 15(4), 57–63 (2000).
[6] Shadow Robot Company. "Developments in Dextrous Hands for Advanced Applications," **In:** *Proceedings of World Automation Congress*, Seville, Spain, IEEE (2004) pp. 123–128.
[7] F. Lotti, P. Tiezzi, G. Vassura, L. Biagiotti and C. Melchiorri, "UBH 3: An Anthropomorphic Hand with Simplified Endo-Skeletal Structure and Soft Continuous Fingerpads," **In:** Proceedings of 2004 IEEE International Conference on Robotics and Automation, New Orleans, LA, USA, IEEE (vol. **5**, 2004) pp. 4736–4741.
[8] H. Liu, K. Wu, P. Meusel, N. Seitz, G. Hirzinger, M. H. Jin, Y. W. Liu, S. W. Fan, T. Lan, Z. P. Chen, "Multisensory Five-Finger Dexterous Hand: The DLR/HIT Hand II," **In:** *Proceedings of 2008 IEEE/RSJ International Conference on Intelligent Robots and Systems*, Nice, France, IEEE (2008) pp. 3692–3697.
[9] T. Laliberté, L. Birglen and C. M. Gosselin, "Underactuation in robotic grasping hands," *Mach. Intell. Robot. Control* **4**(3), 1–11 (2002).
[10] L. U. Odhner, L. P. Jentoft, M. R. Claffee, N. Corson, Y. Tenzer, R. R. Ma, M. Buehler, R. Kohout, R. D. Howe, A. M. Dollar, "A compliant, underactuated hand for robust manipulation," *Int. J. Robot. Res.* **33**(5), 736–752 (2014).
[11] M. Controzzi, F. Clemente, D. Barone, A. Ghionzoli and C. Cipriani, "The SSSA-MyHand: A dexterous lightweight myoelectric hand prosthesis," *IEEE Trans. Neural Syst. Rehabil. Eng.* **25**(5), 459–468 (2017).
[12] D. Liang and W. Zhang, "PASA-GB hand: A novel parallel and self-adaptive robot hand with gear-belt mechanisms," *J. Intell. Robot. Syst.* **90**(1–2), 3–17 (2018).
[13] Y. J. Kim, H. Song and C. Y. Maeng, "BLT gripper: An adaptive gripper with active transition capability between precise pinch and compliant grasp," *IEEE Robot. Autom. Lett.* **5**(4), 5518–5525 (2020).
[14] C. Luo, S. Yang, W. Zhang, Z. Ren and J. Liang, "MPJ Hand: A Self-Adaptive Underactuated Hand with Flexible Fingers of Multiple Passive Joints," **In:** *Proceedings of 2016 International Conference on Advanced Robotics and Mechatronics,* Macau, China, IEEE (2016) pp. 184–189.
[15] J. So, U. Kim, Y. B. Kim, D. Y. Seok, S. Y. Yang, K. Kim, J. H. Park, S. T. Hwang, Y. J. Gong, H. R. Choi, "Shape estimation of soft manipulator using stretchable sensor," *Cyborg Bionic Syst.* **2021**(1), 159–168 (2021) .
[16] V. Tincani, G. Grioli, M. G. Catalano, M. Garabini, S. Grechi, G. Fantoni and A. Bicchi, "Implementation and Control of the Velvet Fingers: A Dexterous Gripper with Active Surfaces," **In:** *Proceedings of 2013 IEEE International Conference on Robotics and Automation,* Karlsruhe, Germany, IEEE (2013) pp. 2744–2750.
[17] Z. Ren, C. Zhou, S. Xin and N. Tsagarakis, "HERI Hand: A Quasi Dexterous and Powerful Hand with Asymmetrical Finger Dimensions and Under Actuation," **In:** *Proceedings of 2017 IEEE/RSJ International Conference on Intelligent Robots and Systems* (2017) pp. 322–328.
[18] S. Abondance, C. B. Teeple and R. J. Wood, "A dexterous soft robotic hand for delicate in-hand manipulation," *IEEE Robot. Autom. Lett.* **5**(4), 5502–5509 (2020).
[19] Y. Yang, K. Vella and D. P. Holmes, "Grasping with kirigami shells," *Sci. Robot.* **6**(54), eabd6426 (2021).
[20] J. L. Pons, E. Rocon and R. Ceres, "The MANUS-HAND dextrous robotics upper limb prosthesis: Mechanical and manipulation aspects," *Auton. Robot.* **16**(2), 143–163 (2004).
[21] K. Mitsui, R. Ozawa and T. Kou, "An Under-Actuated Robotic Hand for Multiple Grasps," **In:** *Proceedings of 2013 IEEE/RSJ International Conference on Intelligent Robots and Systems,* Tokyo, Japan, IEEE (2013) pp. 5475–5480.
[22] Z. Xu and E. Todorov, "Design of a Highly Biomimetic Anthropomorphic Robotic Hand Towards Artificial Limb Regeneration," **In:** *Proceedings of 2016 IEEE International Conference on Robotics and Automation,* Stockholm, IEEE (2016) pp. 3485–3492.
[23] S. H. Jeong, K. S. Kim and S. Kim, "Designing anthropomorphic robot hand with active dual-mode twisted string actuation mechanism and tiny tension sensors," *IEEE Robot. Autom. Lett.* **16**(3), 1571–1578 (2017).
[24] SRT Gripper. "SFG-FNM2-N5087" (2022). *Available at:* https://softrobottech.com/web/zh/product/238.
[25] B. Calli, A. Walsman, A. Singh, S. Srinivasa and P. Abbeel, "Benchmarking in manipulation research: Using the Yale-CMU-Berkeley object and model set," *IEEE Robot. Autom. Mag.* **22**(3), 36–52 (2015).
[26] Robotiq hand. "3-finger adaptive robot gripper" (2021). *Available at:* https://robotiq.com/products/3-finger-adaptive-robot-gripper.
[27] Barrett hand. "Multi-fingered programmable grasper" (2021). *Available at:* https://advanced.barrett.com/barre%20tthand.

Cite this article: C. Su, R. Wang, T. Lu and S. Wang (2023). "SAU-RFC hand: a novel self-adaptive underactuated robot hand with rigid-flexible coupling fingers", Robotica **41**, 511–529. https://doi.org/10.1017/S0263574722000364